PCCP

RSC Publishing

PAPER

View Article Online
View Journal | View Issue

Towards accurate estimates of the spin-state energetics of spin-crossover complexes within density functional theory: a comparative case study of cobalt(II) complexes†

Cite this: *Phys. Chem. Chem. Phys.*, 2013, **15**, 3752

Alfredo Vargas, Itana Krivokapic, Andreas Hauser and Latévi Max Lawson Daku*

We report a detailed DFT study of the energetic and structural properties of the spin-crossover Co(II) complex $[Co(tpy)_2]^{2+}$ (tpy = 2,2′:6′,2″-terpyridine) in the low-spin (LS) and the high-spin (HS) states, using several generalized gradient approximation and hybrid functionals. In either spin-state, the results obtained with the functionals are consistent with one another and in good agreement with available experimental data. Although the different functionals correctly predict the LS state as the electronic ground state of $[Co(tpy)_2]^{2+}$, they give estimates of the HS–LS zero-point energy difference $\Delta E^{o}_{HL}(tpy)$ which strongly depend on the functional used. This dependency on the functional was also reported for the DFT estimates of the zero-point energy difference $\Delta E^{o}_{HL}(bpy)$ in the HS complex $[Co(bpy)_3]^{2+}$ (bpy = 2,2′-bipyridine) [A. Vargas, A. Hauser and L. M. Lawson Daku, *J. Chem. Theory Comput.*, 2009, **5**, 97]. The comparison of the $\Delta E^{o}_{HL}(tpy)$ and $\Delta E^{o}_{HL}(bpy)$ estimates showed that all functionals correctly predict an increase of the zero-point energy difference upon the bpy → tpy ligand substitution, which furthermore weakly depends on the functionals, amounting to $\Delta(\Delta E^{o}_{HL})_{bpy\rightarrow tpy} \approx +2760\ cm^{-1}$. From these results and basic thermodynamic considerations, we establish that, despite their limitations, current DFT methods can be applied to the accurate determination of the spin-state energetics of complexes of a transition metal ion, or of these complexes in different environments, provided that the spin-state energetics is accurately known in one case. Thus, making use of the availability of a highly accurate *ab initio* estimate of the HS–LS energy difference in the complex $[Co(NCH)_6]^{2+}$ [L. M. Lawson Daku, F. Aquilante, T. W. Robinson and A. Hauser, *J. Chem. Theory Comput.*, 2012, **8**, 4216], we obtain for $[Co(tpy)_2]^{2+}$ and $[Co(bpy)_3]^{2+}$ best estimates of $\Delta E^{o}_{HL}(bpy) \approx -2800\ cm^{-1}$ and $\Delta E^{o}_{HL}(tpy) \approx 0\ cm^{-1}$, in good agreement with the known magnetic behaviour of the two complexes.

Received 3rd December 2012,
Accepted 15th January 2013

DOI: 10.1039/c3cp44336a

www.rsc.org/pccp

1 Introduction

The electronic ground state of Co(II) complexes is either a low-spin (LS) doublet state or a high-spin (HS) quartet state. In octahedral symmetry, these states are the LS $^2E_g(t_{2g}^6e_g^1)$ and HS $^4T_{1g}(t_{2g}^5e_g^2)$ states. When the LS state is the ground state and the excited HS state lies sufficiently close in energy, the Co(II) complexes can exhibit spin crossover (SCO), that is, the entropy-driven thermal transition from the LS state, populated at low temperatures, to the HS state, populated at higher temperatures.[1] The Co(II) SCO complexes constitute a rather small class of SCO complexes,[2,3] especially when compared to their Fe(II) analogues. The title complex, $[Co(tpy)_2]^{2+}$ (tpy = 2,2′:6′,2″-terpyridine), is one of the very first members of this class. Its SCO behaviour was indeed observed as early as in the 1960s.[4,5] The complex is shown in Fig. 1. Its geometry is generally depicted as being of D_{2d} molecular symmetry.

The trigonal complex $[Co(bpy)_3]^{2+}$ (bpy = 2,2′-bipyridine) is usually a HS species, although bpy is considered a stronger ligand than tpy.[6] Actually, in $[Co(tpy)_2]^{2+}$, the coordination motif brought about by the tridentate terimine tpy ligand is believed to be responsible for the stabilization of the LS state with respect to the HS state.[3,6] Indeed, the rigid geometry of tpy

Université de Genève, 30 quai Ernest-Ansermet, CH-1211 Genève 4, Switzerland. E-mail: max.lawson@unige.ch

† Electronic supplementary information (ESI) available: Selected bond lengths and angles characterizing the optimized LS and HS geometries of $[Co(tpy)_2]^{2+}$, values found for the pseudo-Jahn–Teller stabilization energy of LS $[Co(tpy)_2]^{2+}$ and for the tetragonal splitting of the HS state in $[Co(tpy)_2]^{2+}$, results obtained for the study at the OLYP level of the influence of scalar relativistic effects on the LS and HS geometries of $[Co(tpy)_2]^{2+}$, $[Co(bpy)_3]^{2+}$ and $[Co(NCH)_6]^{2+}$ and on their energetics. See DOI: 10.1039/c3cp44336a

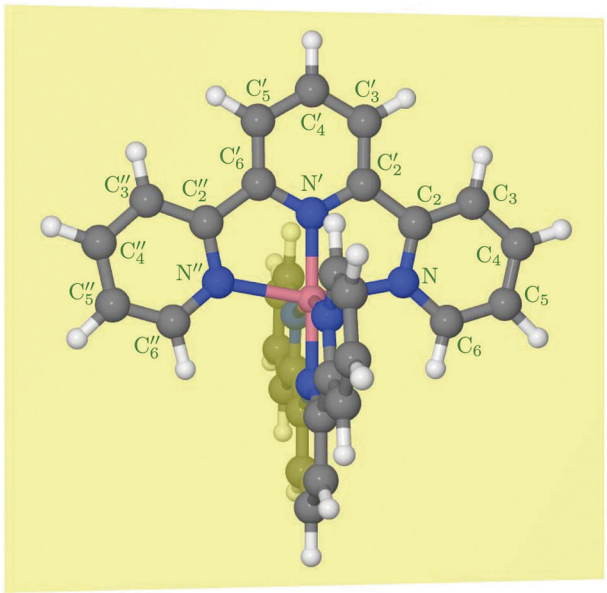

Fig. 1 The $[Co(tpy)_2]^{2+}$ complex. In the D_{2d} and C_{2v} molecular symmetries which will be considered, the tpy ligands are planar and lie in two perpendicular planes. The plane corresponding to the ligand on the top is depicted in yellow. The atom labeling used is also shown.

imposes short axial Co–N bonds and long distal Co–N bonds. The resulting tetragonal compression leads to destabilization of the d_{z^2} component of the antibonding e_g level, which is not favorable to the HS state characterized by two unpaired electrons in the e_g level, but stabilizes one component of the Jahn–Teller (JT) unstable ^2E_g state.

The SCO behaviour of $[Co(tpy)_2]^{2+}$ is strongly influenced by the environment of the complex. It thus proves to be sensitive to the nature of the counteranions, to the nature and number of incorporated solvent molecules in crystalline media, and, in solutions, to the nature of the solvent.[4–18] The magnetic properties of $[Co(bpy)_3]^{2+}$ are also sensitive to the environment of the complex. Indeed, upon the incorporation of $[Co(bpy)_3]^{2+}$ into the supercages of zeolite Y[19–21] or into the cavities of three-dimensional oxalate networks,[22,23] the LS state becomes the ground state and the complex exhibits SCO. This makes the choice of the environment an efficient means for fine tuning the SCO behaviour of the two Co(II) imine complexes. Their behaviour can also be modified chemically, as recently demonstrated with the series of $[Co(tpyRX)_2]^{2+}$ complexes (tpyRX = 4′-alkoxy-2,2′:6′,2″-terpyridine, X = 4, 8, 12), whose SCO behaviour in the solid state proves to depend on the nature of the alkoxy-substituting group and on the nature of the counteranion as well.[24] The detailed characterization of the two isolated Co(II) imine complexes in the two spin states is required for the in-depth understanding of the evolution of their magnetic properties with the environment and upon chemical modification of the ligands. In a previous study,[25] we have characterized within density functional theory (DFT)[26,27] the geometric, energetic and optical properties of $[Co(bpy)_3]^{2+}$ in the HS and Jahn–Teller unstable LS states. In this paper, we extend this DFT study to the $[Co(tpy)_2]^{2+}$ complex.

We will thus characterize the geometric and energetic properties of $[Co(tpy)_2]^{2+}$ in the LS state then in the HS state by carrying out optimization calculations in D_{2d} with different generalized gradient approximation (GGA) and hybrid exchange–correlation (XC) functionals. The LS state of $[Co(tpy)_2]^{2+}$ is however prone to a pseudo-Jahn–Teller (PJT) instability, which may lead to a lowering of the molecular symmetry to C_{2v}.[13] Consequently, for investigating this vibronic instability, we will perform further calculations in C_{2v} for the complex in the LS state. This will involve the determination of the C_{2v} PJT-distorted LS geometry of the complex and the associated PJT stabilization energy. For $[Co(tpy)_2]^{2+}$ in the HS state, we will evaluate the tetragonal splitting of this spin state and examine the extent to which this splitting is influenced by a $D_{2d} \rightarrow C_{2v}$ symmetry lowering.

Finally, we will discuss the performances of the functionals used for the determination of the HS–LS energy differences in $[Co(tpy)_2]^{2+}$ and $[Co(bpy)_3]^{2+}$. Furthermore, from the comparison of the HS–LS energy differences in the two complexes, we will discuss the extent to which DFT methods can be used for the accurate prediction of the variation of the HS–LS energy difference in Co(II) imine complexes and, more generally, in families of transition metal complexes. By extending the comparison to the benchmark complex $[Co(NCH)_6]^{2+}$ for which highly accurate *ab initio* estimates of the HS–LS energy difference have been recently reported,[28] we will make use of our results to derive accurate estimates of this energy difference in $[Co(tpy)_2]^{2+}$ and in $[Co(bpy)_3]^{2+}$.

2 Computational details

The DFT calculations were carried out with the Gaussian 03[29] and the Amsterdam Density Functional (ADF)[30,31] program packages. Both packages were used for the optimization of the LS and HS geometries of the complex and subsequent frequency analyses. With the Gaussian 03 package, these calculations were performed using the PBE,[32] OLYP,[33,34] OPBE[32,34] and HCTH407[35] GGAs, as well as the B3LYP[36,37] and B3LYP*[38,39] hybrids, in combination with the Gaussian-type orbital (GTO) TZVP[40] basis set of triple-ζ polarized quality, hereafter referred to as the $\mathscr{G}$ basis set. With the ADF program package, the optimization and frequency calculations were carried out using the PBE, OPBE, RPBE,[41] OLYP, and BLYP[33,42] GGAs and the $\mathscr{S}_{fc}$ Slater-type orbital (STO) basis set. $\mathscr{S}_{fc}$ consists of the TZP basis set of triple-ζ polarized quality from the ADF STO basis set database, with the atomic core orbitals frozen up to the 1s level for the C and N atoms and up to the 2p level for the Co atom.

The calculations were run nonrelativistically. In ref. 28, scalar relativistic (SR) effects were shown to have a strong influence on the HS–LS electronic energy difference ΔE_{HL}^{el} in the complexes $[Co(NCH)_6]^{2+}$ and $[Fe(NCH)_6]^{2+}$. For both complexes, the SR shift to ΔE_{HL}^{el} was accurately determined from the results of CCSD(T) calculations performed with the second-order Douglas–Kroll–Hess (DKH) method[43–45] extrapolated to the complete basis set limit (CBS(∞)). The SR shifts were found to have a weak dependence on the basis set, and also to be hardly affected by the degree of treatment of electron correlation since the HF and CCSD estimates are very close to the

CCSD(T) best estimates. For $[Co(NCH)_6]^{2+}$, the DKH-CCSD(T)/CBS(∞) estimate of the SR shift is +694 cm^{-1}. In the present study, the influence of SR effects has been probed by carrying out additional optimization calculations for $[Co(tpy)_2]^{2+}$, $[Co(bpy)_3]^{2+}$ and $[Co(NCH)_6]^{2+}$ in the two spin states. The relativistic calculations were run within the zero-order regular approximation (ZORA) for relativistic effects,[46–50] using the ADF program package and the OLYP functional combined with the all-electron ZORA TZP STO basis set from the ADF basis set database. The influence of SR effects on the calculated geometries and on the vibrational contributions to the zero-point energies as well as their differences turned out to be weak (see ESI†). For $[Co(NCH)_6]^{2+}$, the ZORA-OLYP estimate of the SR shift to ΔE_{HL}^{el} is +617 cm^{-1}, in very good agreement with the DKH-CCSD(T)/CBS(∞) value[28] and also with the DKH-PBE value of +608 cm^{-1} (see ESI of ref. 28). Such an agreement shows that SR results obtained with the DKH and ZORA results can be compared in a straightforward manner. For $[Co(bpy)_3]^{2+}$, the calculated SR shift to ΔE_{HL}^{el} is +274 cm^{-1}. For $[Co(tpy)_2]^{2+}$, the influence of SR effects on the energy differences between states of the same spin multiplicities proved to be negligible, and the SR shift to ΔE_{HL}^{el} is +386 cm^{-1}. In the following, the reported energy differences will include the SR shifts thus determined.

All DFT calculations were run unrestricted; with the molecular symmetry constrained to D_{2d} or C_{2v} for $[Co(tpy)_2]^{2+}$, to D_{2h} for $[Co(NCH)_6]^{2+}$,[28] and to C_2 or D_3 for $[Co(bpy)_3]^{2+}$.[25] Molecular visualization was performed with the Jmol program.[51,52]

3 Results and discussion

3.1 Characterization of $[Co(tpy)_2]^{2+}$ in the LS manifold

Upon the $O_h \rightarrow D_{2d}$ symmetry lowering, the ligand-field $^2E_g(t_{2g}^6e_g^1)$ state is split into the $^2B_2$ and $^2A_1$ states characterized by the single occupancy of the metallic antibonding $d_{x^2-y^2}$ and d_{z^2} orbitals of octahedral Co(e_g) parentage, respectively. The calculations performed in D_{2d} give the $^2B_2$ state as the most stable tetragonal component. This agrees with the fact that the tetragonal compression imposed by the ligands destabilizes the d_{z^2} level.

3.1.1 The high-symmetry D_{2d} LS geometry. Selected bond lengths and angles characterizing the calculated LS D_{2d} geometries are summarized in Table 1. Given that the calculated geometries exhibit a weak dependence on the XC functionals used, only average values and standard deviations of the functionals are reported. The full results are available in the ESI.† The values found for these structural parameters in the 120 K X-ray structure of LS $[Co(tpy)_2]I_2{\cdot}2H_2O$[14] are also given in Table 1.

Inspection of Table 1 shows that the ADF and G03 calculated D_{2d} geometries are in good agreement with experiment. Thus, as experimentally observed, the equatorial cobalt–nitrogen bonds are longer than the axial cobalt–nitrogen bonds, and the C–C bonds between the pyridinyl rings are longer than the benzylic C–C bonds (see ESI†). However, the calculated geometries tend to be slightly more expanded than experimentally observed for most optimized bond lengths. This observation does not hold for the Co–N′ bond since, with the exception of the B3LYP/$\mathscr{G}$ and B3LYP*/$\mathscr{G}$ geometries, the calculated geometries exhibit shorter Co–N′ bonds than experimentally observed (see ESI†). Actually, the B3LYP and B3LYP* hybrids give slightly longer cobalt–nitrogen bonds than the GGAs and, in order to understand the difference observed between the experimental and calculated Co–N′ distances, one should rather consider the ratio η of the axial to the distal cobalt–nitrogen bond lengths

$$\eta = \frac{d(\mathrm{Co-N''})}{d(\mathrm{Co-N})}. \quad (1)$$

While η takes for the X-ray structure a value of 0.918, it takes for the calculated geometries values of between 0.891 and 0.902 depending on the functional used. That is, independently of the tendency of the functionals to give more or less long cobalt–nitrogen bonds, they all predict a more pronounced tetragonal compression than experimentally observed.[53] The differences between the experimental and the calculated D_{2d} geometries remain rather small, as also attested by the similar values of the angles α, β and β' which describe the spatial arrangement of the ligands about the metal center (Table 1). They can be ascribed to the neglect of the crystal packing effects in our calculations performed in the gas phase, and also to the neglect of the vibronic instability of the LS state at this stage.

3.1.2 The vibronic instability of the LS state. The vibrational analyses performed on the optimized D_{2d} geometries indicate that the $^2B_2$ state is a first-order transition state, characterized by one imaginary frequency associated with a normal vibration of b_2 symmetry. This instability of the D_{2d}

Table 1 Selected bond lengths (Å) and angles (°) in the optimized LS $^2B_2$ $[Co(tpy)_2]^{2+}$ geometries of D_{2d} symmetry. The reported parameter values are averages over the ADF and G03 calculated structures, with standard deviations given in parentheses. Experimental values are also given for comparison purposes

	Exp.[a]	ADF	G03
Co–N, Co–N″	2.083	2.116(8)	2.115(22)
Co–N′	1.912	1.892(8)	1.895(19)
$\alpha = \angle(C_6' - C_2'', C_2 - C_2')$	106.5	107.5(2)	107.5(6)
$\beta = \angle(N' - Co - N) = \angle(N'' - Co - N')$	79.4	80.1(1)	80.0(3)
$\beta' = \angle(N'' - Co - N)^b$	158.9	160.2(2)	160.0(6)
$\gamma = \angle(N' - C_2' - C_2 - N) = \angle(N'' - C_2'' - C_6' - N')^b$	1.2	0.0	0.0
$\eta = d$(Co–N′)/d(Co–N″)	0.918	0.894(1)	0.896(4)

[a] Data are for the $[Co(tpy)_2]^{2+}$ geometry of approximate D_{2d} symmetry found in the 120 K X-ray structure of LS $[Co(tpy)_2]I_2{\cdot}2H_2O$.[14] [b] The D_{2d} symmetry constraint imposes that $\beta' = 2\beta$ and $\gamma = 0$.

Table 2 Selected bond lengths (Å) and angles (°) in the optimized LS $^2A_1$ $[Co(tpy)_2]^{2+}$ geometries of C_{2v} symmetry, and variations of these structural parameters on going from the LS D_{2d} to the LS C_{2v} geometries. The reported values are averages over the ADF and G03 calculated structures, with standard deviations given in parentheses

	ADF		G03	
	L_1	L_2	L_1	L_2
Values of the selected structural parameters in the optimized LS geometries of C_{2v} symmetry				
Co–N, Co–N″	2.009(11)	2.222(10)	2.012(23)	2.214(22)
Co–N′	1.867(9)	1.961(8)	1.872(19)	1.952(16)
$\alpha = \angle(C'_6 - C''_2,\ C_2 - C'_2)$	103.5(3)	110.9(2)	103.6(6)	110.7(6)
$\beta = \angle(N' - Co - N) = \angle(N'' - Co - N')$	81.3(1)	78.0(1)	81.2(3)	78.3(3)
$\beta' = \angle(N'' - Co - N)^a$	162.5(2)	155.9(2)	162.5(6)	156.5(6)
$\gamma = \angle(N' - C'_2 - C_2 - N) = \angle(N'' - C''_2 - C'_6 - N')^a$	0.0	0.0	0.0	0.0
Structural changes upon the $D_{2d} \rightarrow C_{2v}$ symmetry lowering				
Co–N, Co–N″	−0.107(6)	+0.105(5)	−0.104(3)	+0.098(3)
Co–N′	−0.025(2)	+0.068(3)	−0.024(1)	+0.057(4)
$\alpha = \angle(C'_6 - C''_2,\ C_2 - C'_2)$	−4.0(2)	+3.4(1)	−3.9(1)	+3.2(1)
$\beta = \angle(N' - Co - N) = \angle(N'' - Co - N')$	+1.2(1)	−2.1(1)	+1.2(1)	−1.8(1)
$\beta' = \angle(N'' - Co - N)^a$	+2.3(2)	−4.2(2)	+2.5(2)	−3.5(2)
$\gamma = \angle(N' - C'_2 - C_2 - N) = \angle(N'' - C''_2 - C'_6 - N')^a$	0.0	0.0	0.0	0.0

[a] The C_{2v} symmetry constraint imposes that $\beta' = 2\beta$ and $\gamma = 0$.

configuration of $[Co(tpy)_2]^{2+}$ is due to a pseudo-Jahn–Teller (PJT) effect,[54] that is, the vibronic coupling between the non-degenerate LS ground state and one or several excited doublet states. It is responsible for the distortion of the molecular structure towards an extremum of C_{2v} symmetry, which is given as a true minimum by the vibrational analyses performed on the optimized C_{2v} geometries, and which corresponds to an electronic state of $^2A_1$ symmetry.

The PJT-distorted C_{2v} geometry. Selected bond lengths and angles characterizing the calculated LS C_{2v} geometries are given in Table 2, along with their changes on going from the LS D_{2d} to the LS C_{2v} geometries. Owing to the weak dependence of the optimized geometries on the XC functionals used, only average values and standard deviations over the functionals are reported.

The structural data in Table 2 show that the LS C_{2v} geometries obtained with the G03 and ADF packages are consistent with one another. They also show that the passing from the LS D_{2d} to the LS C_{2v} geometries is mainly characterized by the fact that one ligand, noted L_1, moves closer to the cobalt atom while the other ligand, noted L_2, concomitantly moves away from it. Thus, there is for L_1 a shortening of the equatorial and axial metal–nitrogen bonds of ~0.1 Å and ~0.03 Å, respectively, which is accompanied by a decrease of the angle α of ~4° and an increase of the angle β of ~1° (note that $\beta' = 2\beta$ in D_{2d} and C_{2v}). For L_2, one observes a lengthening of the equatorial and axial metal–nitrogen bonds of ~0.1 Å and ~0.06 Å, respectively, associated with an increase of α of ~3° and a decrease of β of ~2°. The large structural changes thus undergone by the complex are illustrated by the superposition in Fig. 2 of its OLYP/$\mathscr{S}_{fc}$ optimized D_{2d} and C_{2v} geometries.

The PJT stabilization energy and the dynamic nature of the vibronic instability. The different functionals perform very similarly for the calculation of the PJT stabilization energy E_{PJT}:

$$E_{PJT} = E^{el}(^2B_2) - E^{el}(^2A_1). \quad (2)$$

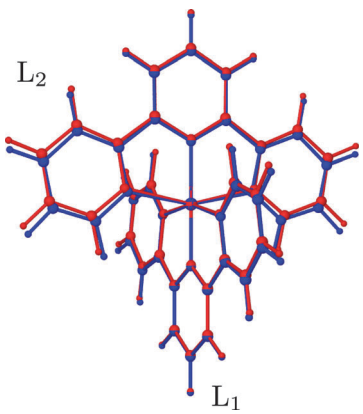

Fig. 2 Superposition of the optimized OLYP/$\mathscr{S}_{fc}$ geometries of $[Co(tpy)_2]^{2+}$ in the LS manifold: LS geometry of D_{2d} symmetry (blue) and PJT-distorted LS geometry of C_{2v} symmetry (red).

They indeed consistently predict that E_{PJT} is small, with calculated values of between 140 cm^{-1} and 240 cm^{-1}, from which a reliable estimate of

$$E_{PJT} = 205(70)\ cm^{-1} \quad (3)$$

is obtained for the PJT stabilization energy (see ESI†).

The tetragonal symmetry of the PJT problem imposes the presence on the LS ground-state adiabatic potential energy surface (APES) of two equivalent C_{2v} minima connected by the D_{2d} $^2B_2$ saddle point. As will be reported elsewhere, the PJT instability is a multimode problem: besides the b_2 vibrational mode of imaginary frequency, many other modes of b_2 and a_1 symmetries contribute to the PJT distortion.[55] Given the small value of E_{PJT}, the PJT instability of the LS state effect is expected to be dynamic for the *isolated* complex. The approximate D_{2d} symmetry of the LS X-ray structure of the complex[14] and the symmetry of the EPR spectrum determined for LS

$[Co(tpy)_2]^{2+}$ from measurements performed at 4.2 K on the SCO system $[Fe_{1-x}Co_x(tpy)_2](PF_6)_2$ (x = 4%)[6,56] suggest that this is also the case in the solid state.

3.2 Characterization of $[Co(tpy)_2]^{2+}$ in the HS manifold

3.2.1 Characterization in D_{2d}. In D_{2d}, the ligand-field $^4T_{1g}(t_{2g}^5e_g^2)$ state is split into the $^4A_2$ and ^4E states which essentially differ by the occupancies of the nonbonding metallic degenerate $e_\downarrow = (d_{xz\downarrow}, d_{yz\downarrow})$ and nondegenerate $b_{1\downarrow} = d_{xy\downarrow}$ spin-down orbitals of octahedral $Co(t_{2g})$ parentage: namely, $(e_\downarrow)^2(b_{1,\downarrow})^1$ and $(b_{1,\downarrow})^2(e_\downarrow)^1$ for the $^4A_2$ and ^4E states, respectively. Because of the difference in their handling of orbitally degenerate states, ADF allowed the characterization of $[Co(tpy)_2]^{2+}$ in both states whereas G03 was restricted to the $^4A_2$ state. The ^4E state is JT unstable, and the calculated $^4A_2$ geometries were given as true minima by the vibrational analyses performed after the optimizations.

Optimized $^4A_2$ and ^4E geometries. The selected bond lengths and angles employed above for the description of the LS geometries are also used for characterizing the HS geometries. The calculated HS structures prove to vary little with the XC functionals. Hence, as was also the case for the LS geometries, only average values and standard deviations of the functionals are reported for the selected structural parameters. They are summarized in Table 3, while the full results are given in the ESI.† We also list in Table 3 the variations of these parameters on going from the LS D_{2d} to the HS D_{2d} geometries.

Inspection of Table 3 shows that the ADF and G03 optimized $^4A_2$ geometries are quite similar and that the HS geometry of $[Co(tpy)_2]^{2+}$ hardly evolves on going into the ^4E state. This is due to the fact that, as stated above, the passing from the $^4A_2$ to the ^4E state mainly involves the transfer of an electron from the nonbonding metallic $b_{1\downarrow} = d_{xy\downarrow}$ level to the nonbonding metallic $e_\downarrow = (d_{xz\downarrow}, d_{yz\downarrow})$ level. Table 3 gives also the values found for the structural parameters in the 295 K X-ray structure of HS $[Co(tpy)_2](ClO_4)_2{\cdot}1.3H_2O$.[15] The comparison of these values with those reported for the optimized geometries indicates that these agree quite well with the experimental ones,[15] all the more so as the HS fraction of the perchlorate salt at room temperature is actually around 80% only.[57] The ratio η of the central to the distal cobalt–nitrogen bond lengths takes a value of 0.949 for the HS X-ray structure and, for the calculated geometries, values of between 0.933 and 0.947 depending on the functional used. The functionals therefore tend to predict a tetragonal coordination which is slightly more compressed than observed. The tetragonal compression observed for D_{2d} $[Co(tpy)_2]^{2+}$ in the HS states is less marked than in the LS state, wherein η = 0.918 for the experimental LS geometry and η = 0.891–0.902 for the calculated D_{2d} LS geometries. This is due to the fact that the LS → HS change of spin-states is accompanied by an increase of the axial and distal cobalt–nitrogen bond lengths of *ca.* 0.12 Å and 0.05 Å, respectively, for the X-ray structures, and of *ca.* 0.16 Å and 0.05 Å, respectively, for the optimized structures. As the ligands move away from the central metal ion, the bite angle β and $\beta' = 2\beta$ is predicted to decrease by about 3.5° and 7°, respectively, in agreement with experiment. The driving force of the strongly anisotropic dilatation of the coordination sphere upon the LS → HS change of spin-states is the promotion of one electron from the nonbonding metallic levels of $Co(t_{2g})$ parentage into the antibonding metallic d_{z^2} level of $Co(e_g)$ parentage.

Tetragonal splitting of the HS state. The different functionals give positive values for the tetragonal splitting of the HS state Δ_{HS} defined by the electronic energy difference:

$$\Delta_{HS} = E^{el}(^4E) - E^{el}(^4A_2). \quad (4)$$

The $^4A_2$ state is thus predicted to be the most stable tetragonal component of the HS state, whatever the XC functional used.

Table 3 Selected bond lengths (Å) and angles (°) in the optimized HS $^4A_2$ and ^4E $[Co(tpy)_2]^{2+}$ geometries of D_{2d} symmetry, and associated HS–LS differences. The reported values are averages over the ADF and G03 calculated structures, with standard deviations given in parentheses. Experimental values are also given

		$^4A_2$		^4E
	Exp.[a]	ADF	G03	ADF
Values of the selected structural parameters				
Co–N, Co–N″	2.137	2.179(11)	2.185(16)	2.182(10)
Co–N′	2.028	2.054(10)	2.053(19)	2.062(9)
$\alpha = \angle(C'_6 - C''_2,\ C_2 - C'_2)$	107.5	107.9(3)	107.9(1)	108.0(1)
$\beta = \angle(N' - Co - N) = \angle(N'' - Co - N')$	76.8	76.5(1)	76.6(3)	76.2(1)
$\beta' = \angle(N'' - Co - N)^b$	153.6	153.1(2)	153.2(6)	152.4(2)
$\gamma = \angle(N' - C'_2 - C_2 - N) = \angle(N'' - C''_2 - C'_6 - N')^b$	2.7	0.0	0.0	0.0
$\eta = d(Co–N')/d(Co–N)$	0.949	0.941(2)	0.940(6)	0.945(2)
Variations of the parameters on going from the LS D_{2d} to the HS D_{2d} geometries				
Co–N, Co–N″	+0.053	+0.066(4)	+0.066(12)	+0.069(12)
Co–N′	+0.116	+0.161(3)	+0.169(3)	+0.157(3)
$\alpha = \angle(C'_6 - C''_2,\ C_2 - C'_2)$	+1.0	+0.3(1)	+0.5(4)	+0.4(4)
$\beta = \angle(N' - Co - N) = \angle(N'' - Co - N')^b$	−2.7	−3.5(1)	−3.9(1)	−3.4(1)
$\beta' = \angle(N'' - Co - N)^b$	−5.4	−7.0(2)	−7.8(2)	−6.8(2)
$\gamma = \angle(N' - C'_2 - C_2 - N) = \angle(N'' - C''_2 - C'_6 - N')^b$	+1.5	0.0	0.0	0.0
$\eta = d(Co–N')/d(Co–N)$	+0.031	+0.047(1)	+0.051(4)	+0.044(4)

[a] Data are for the geometry of approximate D_{2d} symmetry found in the 295 K X-ray structure of HS $[Co(tpy)_2](ClO_4)_2{\cdot}1.3H_2O$.[15] [b] The D_{2d} symmetry constraint imposes that $\beta' = 2\beta$ and $\gamma = 0$.

Furthermore, these values are quite consistent with one another (see ESI†), which allows us to propose for Δ_{HS} a reliable estimate of:

$$\Delta_{HS} = +540(110)\ cm^{-1}. \quad (5)$$

The tetragonal splitting thus predicted for the HS ligand-field state is relatively small, especially when compared to the tetragonal splitting of the LS ligand-field state, which gives rise to an intraconfigurational d–d transition with an energy of $\sim$7500 cm^{-1}.[6,13] The fact that Δ_{HS} is small is due to the essentially nonbonding character of the metallic orbital levels involved in the electronic rearrangement accompanying the $^4A_2 \leftrightarrow {}^4E$ change of states.

3.2.2 Splitting of the ligand-field HS state: a more complex picture. A small tetragonal splitting was also determined from the analysis within ligand field theory of the EPR spectrum of the HS complex, recorded at 4.2 K on the HS compound $[Zn_{1-x}Co_x(tpy)_2](PF_6)_2$ (x = 2).[6] In this case however, the ^4E state was found to be the most stable HS component with an experimental estimate of $\Delta_{HS} \approx -600\ cm^{-1}$. In order to understand why the DFT and LFT estimates of Δ_{HS} are of opposite signs, we have examined the possible influence of the JT instability of the ^4E state on the splitting of the ligand-field HS state. For this, we have also optimized the geometry of the HS complex in C_{2v}, knowing that, upon the $D_{2d} \rightarrow C_{2v}$ symmetry lowering, the two HS tetragonal components evolve as follows: $^4E \rightarrow {}^4B_1 \oplus {}^4B_2$ and $^4A_2 \rightarrow {}^4A_2$. Actually, the extrema of the HS APES associated with the HS $^4B_1$ and $^4B_2$ states are equivalent in that their electronic configurations differ only by the occupancies of the equivalent metal-centered orbitals of $3d_{xz}$ and $3d_{yz}$ types and of b_1 and b_2 symmetries, respectively.[58] Finally, the optimizations in C_{2v} were performed for the HS $^4A_2$ and $^4B_1$ states at the OLYP/$\mathscr{S}_{fc}$, OPBE/$\mathscr{S}_{fc}$, RPBE/$\mathscr{S}_{fc}$, BLYP/$\mathscr{S}_{fc}$ and PBE/$\mathscr{S}_{fc}$ levels. Vibrational analyses performed on the optimized geometries indicate that the located C_{2v} extrema correspond to true minima on the HS APES. The equivalent roles of the two terpyridine ligands impose that there actually exist two equivalent $^4A_2$ C_{2v} minima.

The HS C_{2v} geometries obtained with the different functionals are consistent with one another. Selected structural parameters characterizing them are given in the ESI.† Their averages over the calculated structures and those of their variations upon the $D_{2d} \rightarrow C_{2v}$ symmetry lowering are reported in Table 4. Our results indicate that the $^4A_2$ D_{2d} and $^4A_2$ C_{2v} minima do not necessarily coincide (Table 4) but that they are quasi degenerate, their electronic energy difference being less than 10 cm^{-1} whatever the functional used. The $^4B_1$ minimum, hence the equivalent $^4B_2$ minimum also, are found to lie lower in energy than the $^4A_2$ minima, with electronic energy differences of 283, 143, 183, 255 and 132 cm^{-1} calculated at the OLYP/$\mathscr{S}_{fc}$, OPBE/$\mathscr{S}_{fc}$, RPBE/$\mathscr{S}_{fc}$, BLYP/$\mathscr{S}_{fc}$ and PBE/$\mathscr{S}_{fc}$ levels, respectively. The consistency among these predicted energy differences allows us to propose for the electronic difference in C_{2v}

$$\Delta'_{HS} = E^{el}(^4B_{1,2}) - E^{el}(^4A_2) \quad (6)$$

a best estimate of

$$\Delta'_{HS} = -200(70)\ cm^{-1}, \quad (7)$$

and for the JT stabilization energy associated with the vibronic instability of the HS ^4E state given by

$$E_{JT} = \Delta_{HS} - \Delta'_{HS}, \quad (8)$$

a best estimate of

$$E_{JT} = 740(130)\ cm^{-1}. \quad (9)$$

From the above results, we can draw the conclusion (i) that, for the D_{2d} $[Co(tpy)_2]^{2+}$ complex, the HS $^4A_2$ state would be more stable than the HS ^4E state, and (ii) that the electronic state

Table 4 Selected bond lengths (Å) and angles (°) in the optimized HS $^4A_2$ and $^4B_1$ $[Co(tpy)_2]^{2+}$ geometries of C_{2v} symmetry, and their variations upon the D_{2d} to C_{2v} symmetry lowering in the HS states. The reported values are averages over the ADF calculated structures, with standard deviations given in parentheses

	$^4A_2$ in C_{2v}		$^4B_1$ in C_{2v}	
	L_1	L_2	L_1	L_2
Values of the selected structural parameters				
Co–N, Co–N″	2.174(19)	2.197(20)	2.170(21)	2.198(22)
Co–N′	2.047(17)	2.068(16)	2.098(15)	2.064(13)
$\alpha = \angle(C'_6 - C''_2,\ C_2 - C'_2)$	107.5(5)	108.2(4)	107.6(5)	108.2(6)
$\beta = \angle(N' - Co - N) = \angle(N'' - Co - N')$	76.8(3)	76.2(2)	74.9(2)	76.5(3)
$\beta' = \angle(N'' - Co - N)^a$	153.6(6)	152.4(4)	149.8(4)	153.0(6)
$\gamma = \angle(N' - C'_2 - C_2 - N) = \angle(N'' - C''_2 - C'_6 - N')^a$	0.0	0.0	0.0	0.0
Variations associated with the $D_{2d} \rightarrow C_{2v}$ symmetry lowering: $^4A_2 \rightarrow {}^4A_2$ and $^4E \rightarrow {}^4B_1 \oplus {}^4B_2$				
Co–N, Co–N″	−0.008(11)	+0.015(11)	−0.012(12)	+0.016
Co–N′	−0.006(8)	+0.015(6)	+0.037(7)	+0.003
$\alpha = \angle(C'_6 - C''_2,\ C_2 - C'_2)$	−0.2(4)	+0.4(3)	−0.4(4)	+0.2(5)
$\beta = \angle(N' - Co - N) = \angle(N'' - Co - N')$	+0.2(2)	−0.4(2)	−1.3(2)	+0.3(3)
$\beta' = \angle(N'' - Co - N)^a$	+0.4(4)	−0.8(4)	−2.6(4)	+0.6(6)
$\gamma = \angle(N' - C'_2 - C_2 - N) = \angle(N'' - C''_2 - C'_6 - N')^a$	0.0	0.0	0.0	0.0

[a] The C_{2v} symmetry constraint imposes that $\beta' = 2\beta$ and $\gamma = 0$.

actually probed by EPR spectroscopy results from the JT instability of the HS ^{4}E state.

3.3 The HS–LS energy difference in cobalt(II) imine complexes

In order to observe SCO in a Co(II) complex, a prerequisite is that the LS state is its electronic ground state. That is, its HS–LS zero-point energy difference

$$\Delta E^{o}_{HL} = E^{o}_{HS} - E^{o}_{LS} \quad (10)$$

must be positive. The zero-point energy E^{o}_{Γ} of the Γ spin-state (Γ = HS, LS) is given by

$$E^{o}_{\Gamma} = E^{el}_{\Gamma} + E^{vib}_{\Gamma}, \quad (11)$$

where E^{el}_{Γ} is the electronic contribution obtained from the minimization of the energy of the complex in the Γ state, and E^{vib}_{Γ} is the vibrational contribution obtained from the vibration analysis performed within the harmonic approximation. The HS–LS zero-point energy can thus be expressed as the sum of an electronic contribution, $\Delta E^{el}_{HL} = E^{el}_{HS} - E^{el}_{LS}$, and a vibrational contribution, $\Delta E^{vib}_{HL} = E^{vib}_{HS} - E^{vib}_{LS}$:

$$\Delta E^{o}_{HL} = \Delta E^{el}_{HL} + \Delta E^{vib}_{HL}. \quad (12)$$

3.3.1 The $[Co(tpy)_2]^{2+}$ complex. For $[Co(tpy)_2]^{2+}$ in the PJT-unstable LS state, the relevant zero-point energy is the one determined at the PJT-distorted C_{2v} minima: $E^{o}_{LS} = E^{o}(^2A_1)$.[59] For the HS zero-point energy, we have chosen to use that of the $^4A_2$ tetragonal D_{2d} component of the HS state: $E^{o}_{HS} = E^{o}(^4A_2)$. Other choices can of course be made among the C_{2v} minima, which have been located on the HS APES (see above). However, the HS C_{2v} and D_{2d} $^4A_2$ states have the same E^{el} value, which is only $|\Delta'_{HS}| = 200\,cm^{-1}$ larger than the one of the HS C_{2v} $^4B_1$ and $^4B_2$ states. Furthermore, at any of the theoretical levels used for characterizing the splitting of the HS state, the E^{vib} values calculated at the HS D_{2d} and C_{2v} minima are very similar, with the largest difference of 57 cm^{-1} observed for the OLYP/$\mathscr{S}_{fc}$ calculations (data not shown). This probably reflects the fact that going from one of these HS states to another one involves mainly an electronic rearrangement in essentially nonbonding metal-centered orbitals of octahedral t_{2g} parentage. Finally, from the above remarks, it is clear that the choice made by us for the definition of the HS zero-point energy does not introduce any hidden bias in the study of the spin-state energetics of $[Co(tpy)_2]^{2+}$.

Table 5 gives the calculated values of ΔE^{o}_{HL} and of the contributions ΔE^{el}_{HL} and ΔE^{vib}_{HL}. The nearly identical results obtained with the OLYP, OPBE and PBE functionals using the $\mathscr{S}_{fc}$ and $\mathscr{G}$ basis sets show that the two basis sets are of very similar quality and that the results obtained with either basis set can be compared in a straightforward manner. The calculated ΔE^{o}_{HL} values are all positive: the LS state is thus predicted by all functionals to be the electronic ground state of the SCO $[Co(tpy)_2]^{2+}$ complex. However, the ΔE^{o}_{HL} values vary between 202 cm^{-1} and 5947 cm^{-1} depending on the functional used. Furthermore, the strong sensitivity of the magnetic behaviour of $[Co(tpy)_2]^{2+}$ to its environment tends to preclude any comparison between experiment and theory, which could help discriminate between these gas-phase values of ΔE^{o}_{HL} and thus assess the performance of the functionals.

Table 5 Calculated values of ΔE^{o}_{HL} in $[Co(tpy)_2]^{2+}$ and of the contributions ΔE^{el}_{HL} and ΔE^{vib}_{HL}, in cm^{-1}

Theoretical level	ΔE^{o}_{HL}	ΔE^{el}_{HL}	ΔE^{vib}_{HL}
B3LYP/$\mathscr{G}$	+588	+762	−174
B3LYP*/$\mathscr{G}$	+2042	+2223	−181
HCTH407/$\mathscr{G}$	+2351	+2530	−179
OLYP/$\mathscr{G}$	+3317	+3487	−170
OLYP/$\mathscr{S}_{fc}$	+3413	+3593	−180
OPBE/$\mathscr{S}_{fc}$	+4095	+4236	−141
OPBE/$\mathscr{G}$	+4136	+4283	−147
RPBE/$\mathscr{S}_{fc}$	+4574	+4785	−211
BLYP/$\mathscr{S}_{fc}$	+5594	+5810	−216
PBE/$\mathscr{G}$	+6289	+6456	−167
PBE/$\mathscr{S}_{fc}$	+6333	+6536	−203

Inspection of Table 5 shows that the values found for ΔE^{vib}_{HL} depend only weakly on the theoretical level used, with average and standard deviation of these values of −183 cm^{-1} and 23 cm^{-1}, respectively. This allows us to give for this quantity an accurate estimate of

$$\Delta E^{vib}_{HL} = -185(25)\ cm^{-1}. \quad (13)$$

Hence, the large spread of the calculated ΔE^{o}_{HL} values clearly originates from the electronic component ΔE^{el}_{HL} since $762\ cm^{-1} \leq \Delta E^{el}_{HL} \leq 6536\ cm^{-1}$. These results illustrate the difficulties met with the approximate XC functionals for the determination of the electronic energy difference between states of different spin multiplicities of transition metal complexes. This issue has received tremendeous attention.[25,28,38,39,60–94] But so far, none of the available XC functional could be established as the functional of choice for the evaluation of ΔE^{el}_{HL}. The results obtained for $[Co(tpy)_2]^{2+}$ illustrate the trends generally observed among the functionals. Hybrid functionals tend to lead to an underestimation of ΔE^{el}_{HL}, and ΔE^{el}_{HL} decreases with the amount of included Hartree–Fock (HF) exchange, as can be seen from the results obtained with the B3LYP and B3LYP* hybrids which differ only by the amount of admixed HF exchange of 20% and 15%, respectively. In contrast, semilocal functionals such as the GGAs tend to lead to an overestimation of ΔE^{el}_{HL}. We will not discuss further this delicate issue. In the following, we will rather focus on what can be accurately done for the spin-state energetics of Co(II) imine complexes within the limitations of the current approximations to the true XC functional.

3.3.2 $[Co(bpy)_3]^{2+}$ *versus* $[Co(tpy)_2]^{2+}$: an instructive comparison. The $[Co(bpy)_3]^{2+}$ complex is a HS species when not chemically confined in a tight fitting environment,[6,19–23] which we have recently thoroughly characterized within DFT.[25] We used the GTO $\mathscr{G}$ and STO $\mathscr{S}_{ae}$ basis sets, the latter being the all-electron counterpart of $\mathscr{S}_{fc}$. The hybrid GGA and meta-GGA functionals used gave consistent results for the geometries of the trigonal complex $[Co(bpy)_3]^{2+}$ in the HS and LS states, for the JT instability in the LS state, and for the trigonal splitting of the HS state, and a good agreement between experiment and theory was observed whenever the comparison could be made.

Table 6 Calculated values (cm^{-1}) of ΔE^{el}_{HL} in $[Co(bpy)_3]^{2+}$ and $[Co(tpy)_2]^{2+}$, noted $\Delta E^{el}_{HL}(bpy)$ and $\Delta E^{el}_{HL}(tpy)$, respectively, and of their difference $\Delta(\Delta E^{el}_{HL})_{bpy\rightarrow tpy}$[a]

Functional	Basis type	$\Delta E^{el}_{HL}(bpy)$	$\Delta E^{el}_{HL}(tpy)$	$\Delta(\Delta E^{el}_{HL})_{bpy\rightarrow tpy}$
B3LYP	GTO	−1802	+762	+2564
B3LYP*	GTO	−269	+2223	+2492
HCTH407	GTO	−322	+2530	+2852
OLYP	STO	+608	+3593	+2985
OPBE	STO	+1167	+4236	+3069
RPBE	STO	+1800	+4785	+2985
PBE	GTO	+4110	+6456	+2346
PBE	STO	+4193	+6536	+2343

[a] The $\Delta E^{el}_{HL}(bpy)$ values are the sums of nonrelativistic values taken from ref. 25 and of the scalar relativistic correction (see computational details, Section 2), and the $\Delta E^{el}_{HL}(tpy)$ values are from this work (Table 5). For $[Co(bpy)_3]^{2+}$, in ref. 25, the GTO basis set used is $\mathscr{G}$, and the STO basis set is $\mathscr{S}_{ae}$, the all-electron equivalent of $\mathscr{S}_{fc}$.

Regarding the determination of its HS–LS zero-point energy difference $\Delta E^{o}_{HL}(bpy)$, the vibrational contribution $\Delta E^{vib}_{HL}(bpy)$ was shown to exhibit a weak dependence on the functionals used, as in the present study of $[Co(tpy)_2]^{2+}$, and an estimate of

$$\Delta E^{vib}_{HL}(bpy) \approx -200\ cm^{-1} \quad (14)$$

could thus be given. Note that, from here on, the notation $X(L)$ will be used to designate the value of the quantity X in the Co(II) "L" complex. $\Delta E^{o}_{HL}(bpy)$ itself could not be determined because of the difficulties met with the functionals for the calculation of its electronic contribution $\Delta E^{el}_{HL}(bpy)$. Table 6 allows the comparison of the values found for $\Delta E^{el}_{HL}(bpy)$ and $\Delta E^{el}_{HL}(tpy)$ with the functionals employed in the present study.

Inspection of Table 6 shows that, whatever the functional used, the HS state is predicted to be destabilized with regard to the LS state upon the bpy → tpy ligand substitution. This result is in agreement with the fact that $[Co(bpy)_3]^{2+}$ and $[Co(tpy)_2]^{2+}$ are HS and SCO species, respectively. Furthermore, the values obtained with all functionals for the change in ΔE^{el}_{HL}:

$$\Delta(\Delta E^{el}_{HL})_{bpy\rightarrow tpy} = \Delta E^{el}_{HL}(tpy) - \Delta E^{el}_{HL}(bpy), \quad (15)$$

are very consistent with one another, averaging to +2756 cm^{-1} with a standard deviation of 285 cm^{-1} which falls within the chemical accuracy of 350 cm^{-1}. This allows us to propose for $\Delta(\Delta E^{el}_{HL})_{bpy\rightarrow tpy}$ an accurate estimate of

$$\Delta(\Delta E^{el}_{HL})_{bpy\rightarrow tpy} = +2760(290)\ cm^{-1}. \quad (16)$$

Given that the comparison of eqn (16) and (13) gives

$$\Delta E^{vib}_{HL}(bpy) \approx \Delta E^{vib}_{HL}(tpy), \quad (17)$$

we have for the change in the HS–LS zero-point energy difference

$$\Delta(\Delta E^{o}_{HL})_{bpy\rightarrow tpy} \approx \Delta(\Delta E^{el}_{HL})_{bpy\rightarrow tpy} \approx +2760(290)\,cm^{-1}. \quad (18)$$

Hence the accurate knowledge of either of the HS–LS zero-point energy differences, $\Delta E^{o}_{HL}(bpy)$ or $\Delta E^{o}_{HL}(tpy)$, allows the determination of the other one. Unfortunately, this is not the case yet.

We however know that $\Delta E^{o}_{HL}(bpy) \lesssim 0 \lesssim \Delta E^{o}_{HL}(tpy)$: $[Co(bpy)_3]^{2+}$ is indeed a HS species and the magnetic behavior of $[Co(tpy)_2]^{2+}$ is strongly influenced by its environment. It thus follows that

$$-2760\,cm^{-1} \lesssim \Delta E^{o}_{HL}(bpy) \lesssim 0 \lesssim \Delta E^{o}_{HL}(tpy) \lesssim +2760\,cm^{-1}. \quad (19)$$

3.3.3 Toward an accurate determination in DFT of the HS–LS energy differences in classes of transition metal complexes: rationale. The results obtained above for the comparison of the spin-state energetics of $[Co(bpy)_3]^{2+}$ and $[Co(tpy)_2]^{2+}$ suggest that DFT methods can be used for the accurate prediction of the variation of the HS–LS energy differences in Co(II) imine complexes. This proposal can be put on firm ground by making use of the "Born–Haber" cycle of Fig. 3.

This thermodynamic cycle shows that the change in the HS–LS Gibbs free energy differences in two Co(II) complexes, $\left[Co^{II}(L_a)_{n_a}\right]^{q_a}$ and $\left[Co^{II}(L_b)_{n_b}\right]^{q_b}$,

$$\Delta(\Delta G^{o}_{HL})_{L_a\rightarrow L_b} = \Delta G^{o}_{HL}(L_b) - \Delta G^{o}_{HL}(L_a) \quad (20)$$

can be determined from the knowledge of the standard Gibbs free energy differences $\Delta_r G^{o}_{\Gamma}(L_a \rightarrow L_b)$, ($\Gamma$ = LS, HS) associated with the $L_a \rightarrow L_b$ ligand substitutions in the two spin states, using the relation:

$$\Delta(\Delta G^{o}_{HL})_{L_a\rightarrow L_b} = \Delta_r G^{o}_{HS}(L_a \rightarrow L_b) - \Delta_r G^{o}_{LS}(L_a \rightarrow L_b). \quad (21)$$

The above equality reduces in the $T \rightarrow 0$ limit to an identical equality between zero-point energy differences. It clearly shows

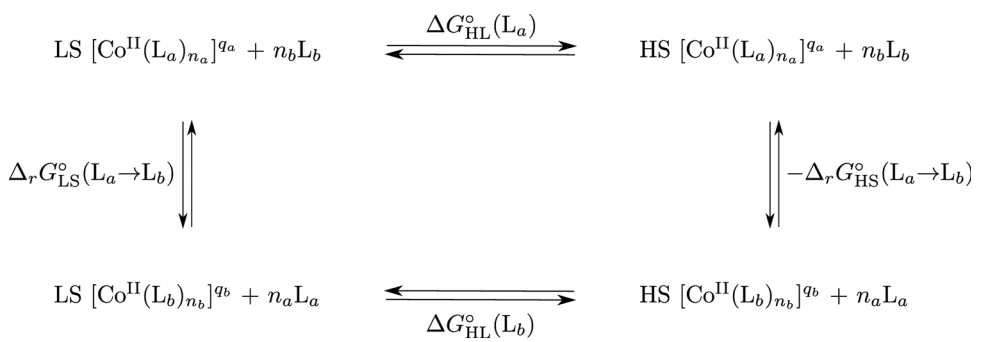

Fig. 3 Free energy "Born–Haber" cycle for the determination of $\Delta(\Delta G^{o}_{HL})_{L_a\rightarrow L_b}$.

that the change in the spin-state energetics or, equivalently, in the thermodynamics of the LS ⇆ HS equilibrium of a Co(II) complex upon a ligand exchange reaction, can be accurately described by any approximate XC functional able to describe the thermochemistry of the substitution reaction in the two spin states accurately. This tends to be the case for most modern functionals. This will be all the more true for exchanged ligands which are chemically related, as in the case of the imine tpy and bpy ligands.

DFT methods can thus be applied to the accurate prediction of the variation of the spin-state energetics or thermodynamics of the LS ⇆ HS equilibrium in classes of transition metal complexes. There is *a priori* no restriction neither on the homoleptic or heteroleptic character of the considered complexes, nor on the nature of the transition metal. For instance, Zein *et al.*[77] have reported that the variation of the HS–LS energy difference in two iron(II) SCO complexes could be correctly described by almost all the 53 functionals, which they have assessed.

Our reasoning based on the use of a Born–Haber cycle readily extends to any two complexes of a given transition metal ion M^{n+}. Hence, denoting $\mathscr{E}_a$ and $\mathscr{E}_b$ the chemically distinct coordination environments of M^{n+} in the two complexes, the equality given by eqn (21) can be rewritten to take the most general form:

$$\Delta\left(\Delta G^{o}_{HL}\right)_{\mathscr{E}_a\rightarrow\mathscr{E}_b} = \Delta_r G^{o}_{HS}(\mathscr{E}_a \rightarrow \mathscr{E}_b) - \Delta_r G^{o}_{LS}(\mathscr{E}_a \rightarrow \mathscr{E}_b). \quad (22)$$

$\Delta\left(\Delta G^{o}_{HL}\right)_{\mathscr{E}_a\rightarrow\mathscr{E}_b}$ is the variation of the HS–LS Gibbs free energy difference entailed by the $\mathscr{E}_a \rightarrow \mathscr{E}_b$ chemical modification of the coordination environment of M^{n+}, and $\Delta_r\left(\Delta G^{o}_{\Gamma}\right)_{\mathscr{E}_a\rightarrow\mathscr{E}_b}$ (Γ = LS, HS) are the standard Gibbs free energy changes associated with the modification of the coordination environment in the two spin states. Eqn (22) states that $\Delta\left(\Delta G^{o}_{HL}\right)_{\mathscr{E}_a\rightarrow\mathscr{E}_b}$ can be correctly predicted by all DFT methods which describe the thermochemistry of the $\mathscr{E}_a \rightarrow \mathscr{E}_b$ chemical modification in both spin states accurately.

The considered chemical modifications may also concern the outer coordination sphere of the complex. So, we have recently shown that the variation of the HS–LS energy difference in $[Fe(bpy)_3]^{2+}$ upon its encapsulation in the supercage of zeolite Y could be correctly described by all the GGA and hybrid functionals used.[88] The analysis of the guest–host interactions brought about by the encapsulation showed that, at fixed geometry of the inclusion compound $[Fe(bpy)_3]^{2+}$@Y, these interactions depend neither on the spin state of the dication nor on its nature. They could be identified as the closed-shell interactions between the first coordination sphere defined by the bpy ligands, and the second coordination sphere defined by the supercage, under the polarizing influence of the transition metal dication. The ability of modern functionals to accurately describe such closed-shell interactions explains their good performances for the accurate description of the influence of the encapsulation in zeolite Y on the spin-state energetics of $[Fe(bpy)_3]^{2+}$.

The conclusions drawn from the study of $[Fe(bpy)_3]^{2+}$@Y and those from the comparison between the spin-state energetics of $[Co(tpy)_2]^{2+}$ and $[Co(bpy)_3]^{2+}$ suggest that, when analyzing the issue of the accurate determination of the spin-state energetics of complexes of a given transition metal ion, we may to some extent distinguish between (1) the changes which are taking place at the metal center and (2) those involving their surroundings. (1) A spin-state conversion is accompanied by an increase or a decrease of the spin polarization, which is mainly localized on the transition metal ion, and by a lengthening or shortening of the metal–ligand bonds, which is due to a change in the occupation of the antibonding 3d orbitals of octahedral e_g parentage. The changes in the metal–ligand bonding in either spin state actually tend to be well described within DFT, but this is not the case for the interactions between the localized 3d electrons. (2) The surroundings of the transition metal ion must adapt to the change of spin states so as to keep the metal–ligand bonding interactions optimal. DFT methods tend as well to correctly describe the interactions between the main-group fragments, which usually define the environment of the transition metal ion. Furthermore, in this field of main-group thermochemistry, noticeable progress is continuously being made in DFT, even in the delicate cases of weak interactions.[95]

So, although the calculation in DFT of the HS–LS energy difference in a first-row transition metal complex suffers from the difficulties met by the functionals to correctly account for the changes in the interactions between the localized 3d electrons, eqn (22) shows that advantage can be taken of the good performance of the functionals for the description of the metal–ligand bonding and of the interactions occurring in the coordination environment of the metal to accurately evaluate within DFT the variation of this energy difference among complexes of the transition metal ion. Then, knowing accurately the value of the HS–LS energy difference in a single reference case would allow us to deduce the values in other cases.

3.3.4 Accurate estimates of ΔE^{o}_{HL} in $[Co(tpy)_2]^{2+}$ and $[Co(bpy)_3]^{2+}$. We have recently reported for the benchmark complex $[Co(NCH)_6]^{2+}$ an accurate estimate of the HS–LS electronic energy difference of $\Delta E^{el}_{HL} = -3111$ cm^{-1} obtained from the results of intensive scalar-relativistic CCSD(T) calculations extrapolated to the complete basis set limit.[28] In order to be able to apply the approach detailed above, we have calculated ΔE^{o}_{HL} of $[Co(NCH)_6]^{2+}$, $\Delta E^{o}_{HL}(NCH)$, using different density functionals. The results are summarized in Table 7.

The DFT values of $\Delta E^{o}_{HL}(NCH)$ range from -2193 cm^{-1} to $+2960$ cm^{-1}. As expected, such a dispersion of these DFT estimates of $\Delta E^{o}_{HL}(NCH)$ is due to the electronic contribution ΔE^{el}_{HL}, the vibrational contribution taking values between -434 cm^{-1} and -541 cm^{-1} depending on the functional used,

Table 7 Calculated values (cm^{-1}) of ΔE^{o}_{HL} in $[Co(NCH)_6]^{2+}$ and of the energy differences $\Delta(\Delta E^{el}_{HL})_{NCH\rightarrow bpy}$ and $\Delta(\Delta E^{el}_{HL})_{NCH\rightarrow tpy}$

Functional	Basis type	$\Delta E^{o}_{HL}(NCH)$	$\Delta\left(\Delta E^{o}_{HL}\right)_{NCH\rightarrow bpy}$	$\Delta\left(\Delta E^{o}_{HL}\right)_{NCH\rightarrow tpy}$
B3LYP	GTO	−2193	+245	+2809
B3LYP*	GTO	−814	+374	+2866
HCTH407	GTO	−1804	+1278	+4130
OLYP	STO	−610	+1022	+4007
OPBE	STO	+53	+861	+3930
RPBE	STO	+790	+831	+3816
PBE	GTO	+2879	+1024	+3367
PBE	STO	+2960	+991	+3337

with an average value and a standard deviation of -488 cm^{-1} and 35 cm^{-1}, respectively. The variations $\Delta\left(\Delta E^{o}_{HL}\right)_{NCH\rightarrow bpy}$ and $\Delta\left(\Delta E^{o}_{HL}\right)_{NCH\rightarrow tpy}$ of ΔE^{o}_{HL} upon the NCH $\rightarrow$ bpy and the NCH $\rightarrow$ tpy ligand exchange are also reported in Table 7. They take positive values: this is consistent with the fact that NCH is a weak-field ligand while bpy and tpy are stronger-field ligands. Despite the very distinct chemical nature of NCH and of the polypyridine ligands, the values found for $\Delta\left(\Delta E^{o}_{HL}\right)_{NCH\rightarrow bpy}$ and $\Delta\left(\Delta E^{o}_{HL}\right)_{NCH\rightarrow tpy}$ are spread over narrow ranges. Thus, using the *ab initio* value of -3111 cm^{-1} for ΔE^{el}_{HL}(NCH),[28] this allows us to propose

$$\Delta E^{o}_{HL}(bpy) = -2800(370)\ cm^{-1} \quad (23)$$

and

$$\Delta E^{o}_{HL}(tpy) = 0(550)\ cm^{-1} \quad (24)$$

as best estimates of the gas-phase values of ΔE^{o}_{HL} in $[Co(bpy)_3]^{2+}$ and $[Co(tpy)_2]^{2+}$. These estimates satisfactorily obey the inequalities given by eqn (19). Furthermore, the relatively large negative value found for ΔE^{o}_{HL}(bpy) is consistent with the fact that $[Co(bpy)_3]^{2+}$ is usually a HS species, and that a rather tightly confining environment such as those provided by the supercages of zeolite Y[19–21] or by the cavities of three-dimensional oxalate networks[22,23] is required for turning this complex into a SCO complex. As for the value close to zero found for ΔE^{o}_{HL}(tpy), it is consistent with the fact that $[Co(tpy)_2]^{2+}$ is a SCO complex whose magnetic behaviour is strongly sensitive to its environment.[4–18]

4 Conclusion and outlook

DFT has been applied to the in-depth structural and energetic characterization of the d^7 complex $[Co(tpy)_2]^{2+}$ in the LS and the HS states. The geometry of the complex was optimized in both spin states using several GGA and hybrid functionals combined with large triple-ζ polarized basis sets of similar qualities. The optimizations were performed in D_{2d} and also in C_{2v} in order to take into account the vibronic instability of the LS and HS states. In either spin state and for the considered molecular symmetries, the functionals gave results which are consistent with one another and in good agreement with available experimental data. The different functionals used give positive HS–LS zero-point energy differences ΔE^{o}_{HL}(tpy), thus correctly predicting the LS state as the electronic ground state of $[Co(tpy)_2]^{2+}$. However, the calculated ΔE^{o}_{HL}(tpy) values exhibit a very large spread, which results from the difficulties met with the approximate XC functionals for the accurate determination of the electronic energy differences between states of different spin multiplicities in transition metal complexes.

In order to determine how this limitation of the current approximate functionals can be bypassed, we have compared the results obtained for the spin-state energetics of $[Co(tpy)_2]^{2+}$ with those previously reported for $[Co(bpy)_3]^{2+}$.[25] For all functionals, ΔE^{el}_{HL}(tpy) > ΔE^{el}_{HL}(bpy), in agreement with the fact that $[Co(bpy)_3]^{2+}$ and $[Co(tpy)_2]^{2+}$ are usually HS and SCO species, respectively. Furthermore, the increase $\Delta(\Delta E^{el}_{HL})_{bpy\rightarrow tpy}$ of ΔE^{el}_{HL} upon the bpy $\rightarrow$ tpy ligand substitution exhibits a weak dependence on the functionals: $\Delta(\Delta E^{el}_{HL})_{bpy\rightarrow tpy}$ = +2760(290) cm^{-1}. This suggests that DFT methods can be used for the accurate determination of the variation of the spin-state energetics in Co(II) imine complexes. This proposal could be put on firm ground from basic thermodynamic considerations. It actually turns out that, for a transition metal ion M^{n+} in a given coordination environment $\mathscr{E}_a$, the variation $\Delta\left(\Delta G^{o}_{HL}\right)_{E_a\rightarrow E_b}$ of the HS–LS Gibbs free energy difference entailed by the chemical modification $\mathscr{E}_a \rightarrow \mathscr{E}_b$ of its coordination environment can be correctly predicted by all DFT methods, which describe the thermochemistry of the chemical modification in both spin states accurately (eqn (22)). As discussed above, this tends to be true for most modern functionals. Consequently, *DFT can effectively be applied to the accurate determination of the spin-state energetics of complexes of a transition metal ion, provided that the spin-state energetics of one of these complexes are accurately known.*

In this vein, taking advantage of the fact that a highly accurate *ab initio* estimate of the HS–LS electronic difference in the benchmark complex $[Co(NCH)_6]^{2+}$ has recently been reported,[28] we have calculated with different density functionals the variations $\Delta\left(\Delta E^{o}_{HL}\right)_{NCH\rightarrow bpy}$ and $\Delta\left(\Delta E^{o}_{HL}\right)_{NCH\rightarrow tpy}$ of ΔE^{o}_{HL} upon the NCH $\rightarrow$ bpy and the NCH $\rightarrow$ tpy ligand substitution. Despite the very distinct chemical nature of NCH and the polypyridine ligands, the calculated values of $\Delta\left(\Delta E^{o}_{HL}\right)_{NCH\rightarrow bpy}$ and of $\Delta\left(\Delta E^{o}_{HL}\right)_{NCH\rightarrow tpy}$ are spread over narrow ranges. Best estimates of $\Delta E^{o}_{HL}(bpy) = -2800(370)\,cm^{-1}$ and $\Delta E^{o}_{HL}(tpy) = 0(550)\,cm^{-1}$ could thus be determined, in pretty good agreement with the known magnetic behaviours of $[Co(tpy)_2]^{2+}$ and $[Co(bpy)_3]^{2+}$.

So, using the approach emphasized above, we are able to determine within DFT accurate estimates of the HS–LS energy differences in very various Co(II) complexes with a $[CoN_6]$ core. More generally, for any transition metal complex, this approach makes possible the systematic and accurate DFT study of the evolution of its spin-state energetics with the chemical nature of its ligands or with its environment.

Acknowledgements

This work has benefited from the financial support of the Swiss National Science Foundation (Contract 200020-125175). It has also been supported by grants from the Swiss National Supercomputing Centre (CSCS) under project IDs s296 and s103.

References

1 *Spin Crossover in Transition Metal Compounds I–III*, ed. P. Gütlich and H. A. Goodwin, Springer-Verlag, Heidelberg, 2004, vol. 233–235.
2 J. Zarembowitch, *New J. Chem.*, 1992, **16**, 255–267.
3 P. Gütlich and H. A. Goodwin, *Top. Curr. Chem.*, 2004, **234**, 23–47.
4 R. Hogg and R. G. Wilkins, *J. Chem. Soc.*, 1962, 341–350.

5 J. S. Judge and W. A. Baker Jr., *Inorg. Chim. Acta*, 1967, **1**, 68–72.
6 I. Krivokapic, M. Zerara, M. Lawson Daku, A. Vargas, C. Enachescu, C. Ambrus, P. Tregenna-Piggott, N. Amstutz, E. Krausz and A. Hauser, *Coord. Chem. Rev.*, 2007, **251**, 364–378.
7 R. C. Stoufer, D. W. Smith, E. A. Clevenger and T. E. Norris, *Inorg. Chem.*, 1966, **5**, 1167–1171.
8 J. G. Schmidt, W. S. Brey Jr. and R. C. Stoufer, *Inorg. Chem.*, 1967, **6**, 268–271.
9 C. M. Harris, T. N. Lockyer, R. L. Martin, H. R. H. Patil and E. Sinn, *Aust. J. Chem.*, 1969, **22**, 2105–2116.
10 E. N. Maslen, C. L. Raston and A. H. White, *J. Chem. Soc., Dalton Trans.*, 1974, 1803–1807.
11 C. L. Raston and A. H. White, *J. Chem. Soc., Dalton Trans.*, 1976, 7–12.
12 W. Henke and S. Kremer, *Inorg. Chim. Acta*, 1982, **65**, L115–L117.
13 S. Kremer, W. Henke and D. Reinen, *Inorg. Chem.*, 1982, **21**, 3013–3022.
14 B. N. Figgis, E. S. Kucharski and A. H. White, *Aust. J. Chem.*, 1983, **36**, 1527–1535.
15 B. N. Figgis, E. S. Kucharski and A. H. White, *Aust. J. Chem.*, 1983, **36**, 1537–1561.
16 J. K. Beattie, R. A. Binstead, M. T. Kelso, P. D. Favero, T. G. Dewey and D. H. Turner, *Inorg. Chim. Acta*, 1995, **235**, 245–251.
17 H. Oshio, H. Spiering, V. Ksenofontov, F. Renz and P. Gütlich, *Inorg. Chem.*, 2001, **40**, 1143–1150.
18 C. Enachescu, I. Krivokapic, M. Zerara, J. A. Real, N. Amstutz and A. Hauser, *Inorg. Chim. Acta*, 2007, **360**, 3945–3950.
19 K. Mizuno and J. H. Lunsford, *Inorg. Chem.*, 1983, **22**, 3484–3486.
20 S. K. Tiwary and S. Vasudevan, *Chem. Phys. Lett.*, 1997, **277**, 84–88.
21 S. K. Tiwary and S. Vasudevan, *Inorg. Chem.*, 1998, **37**, 5239–5246.
22 R. Sieber, S. Decurtins, H. Stoeckli-Evans, C. Wilson, D. Yufit, J. A. K. Howard, S. C. Capelli and A. Hauser, *Chem.–Eur. J.*, 2000, **6**, 361–368.
23 M. Zerara and A. Hauser, *ChemPhysChem*, 2004, **5**, 395–399.
24 P. Nielsen, H. Toftlund, A. D. Bond, J. F. Boas, J. R. Pilbrow, G. R. Hanson, C. Noble, M. J. Riley, S. M. Neville, B. Moubaraki and K. S. Murray, *Inorg. Chem.*, 2009, **48**, 7033–7047.
25 A. Vargas, M. Zerara, E. Krausz, A. Hauser and L. M. Lawson Daku, *J. Chem. Theory Comput.*, 2006, **2**, 1342–1359.
26 P. Hohenberg and W. Kohn, *Phys. Rev.*, 1964, **136**, B864–B871.
27 W. Kohn and L. J. Sham, *Phys. Rev.*, 1965, **140**, A1133–A1138.
28 L. M. Lawson Daku, F. Aquilante, T. W. Robinson and A. Hauser, *J. Chem. Theory Comput.*, 2012, **8**, 4216–4231.
29 M. J. Frisch, G. W. Trucks, H. B. Schlegel, G. E. Scuseria, M. A. Robb, J. R. Cheeseman, J. A. Montgomery Jr., T. Vreven, K. N. Kudin, J. C. Burant, J. M. Millam, S. S. Iyengar, J. Tomasi, V. Barone, B. Mennucci, M. Cossi, G. Scalmani, N. Rega, G. A. Petersson, H. Nakatsuji, M. Hada, M. Ehara, K. Toyota, R. Fukuda, J. Hasegawa, M. Ishida, T. Nakajima, Y. Honda, O. Kitao, H. Nakai, M. Klene, X. Li, J. E. Knox, H. P. Hratchian, J. B. Cross, C. Adamo, J. Jaramillo, R. Gomperts, R. E. Stratmann, O. Yazyev, A. J. Austin, R. Cammi, C. Pomelli, J. W. Ochterski, P. Y. Ayala, K. Morokuma, G. A. Voth, P. Salvador, J. J. Dannenberg, V. G. Zakrzewski, S. Dapprich, A. D. Daniels, M. C. Strain, O. Farkas, D. K. Malick, A. D. Rabuck, K. Raghavachari, J. B. Foresman, J. V. Ortiz, Q. Cui, A. G. Baboul, S. Clifford, J. Cioslowski, B. B. Stefanov, G. Liu, A. Liashenko, P. Piskorz, I. Komaromi, R. L. Martin, D. J. Fox, T. Keith, M. A. Al-Laham, C. Y. Peng, A. Nanayakkara, M. Challacombe, P. M. W. Gill, B. Johnson, W. Chen, M. W. Wong, C. Gonzalez and J. A. Pople, *Gaussian 03, Revision B.03/B.04*, Gaussian, Inc., Pittsburgh PA, 2003.
30 *Amsterdam Density Functional program*, Theoretical Chemistry, Vrije Universiteit, Amsterdam, the Netherlands. http://www.scm.com (accessed July 23, 2012).
31 G. te Velde, F. M. Bickelhaupt, E. J. Baerends, C. Fonseca Guerra, S. J. A. van Gisbergen, J. G. Snijders and T. Ziegler, *J. Comput. Chem.*, 2001, **22**, 931–967.
32 J. P. Perdew, K. Burke and M. Ernzerhof, *Phys. Rev. Lett.*, 1996, **77**, 3865–3868.
33 C. Lee, W. Yang and R. G. Parr, *Phys. Rev. B: Condens. Matter Mater. Phys.*, 1988, **37**, 785–789.
34 N. C. Handy and A. J. Cohen, *Mol. Phys.*, 2001, **99**, 403–412.
35 A. D. Boese and N. C. Handy, *J. Chem. Phys.*, 2001, **114**, 5497–5503.
36 A. D. Becke, *J. Chem. Phys.*, 1993, **98**, 5648–5652.
37 Gaussian NEWS, v. 5, no. 2, summer 1994, p. 2, *Becke3LYP Method References and General Citation Guidelines*.
38 M. Reiher, O. Salomon and B. A. Hess, *Theor. Chem. Acc.*, 2001, **107**, 48–55.
39 O. Salomon, M. Reiher and B. A. Hess, *J. Chem. Phys.*, 2002, **117**, 4729–4737.
40 A. Schäfer, C. Huber and R. Ahlrichs, *J. Chem. Phys.*, 1994, **100**, 5829–5835.
41 B. Hammer, L. B. Hansen and J. K. Nørskov, *Phys. Rev. B: Condens. Matter Mater. Phys.*, 1999, **59**, 7413–7421.
42 A. D. Becke, *Phys. Rev. A*, 1988, **38**, 3098–3100.
43 M. Douglas and N. M. Kroll, *Ann. Phys.*, 1974, **82**, 89–155.
44 B. A. Hess, *Phys. Rev. A*, 1985, **32**, 756–763.
45 B. A. Hess, *Phys. Rev. A*, 1986, **33**, 3742–3748.
46 J.-L. Heully, I. Lindgren, E. Lindroth, S. Lundqvist and A.-M. Mårtensson-Pendrill, *J. Phys. B: At. Mol. Phys.*, 1986, **19**, 2799–2815.
47 C. Chang, M. Pelissier and P. Durand, *Phys. Scr.*, 1986, **34**, 394–404.
48 E. van Lenthe, E. J. Baerends and J. G. Snijders, *J. Chem. Phys.*, 1993, **99**, 4597–4610.
49 E. van Lenthe, R. van Leeuwen, E. J. Baerends and J. G. Snijders, *Int. J. Quantum Chem.*, 1996, **57**, 281–293.
50 E. van Lenthe, A. Ehlers and E. J. Baerends, *J. Chem. Phys.*, 1999, **110**, 8943–8953.
51 *Jmol: an open-source Java viewer for chemical structures in 3D*, http://www.jmol.org (accessed Feb. 14, 2010).

52 B. McMahon and R. M. Hanson, *J. Appl. Crystallogr.*, 2008, **41**, 811–814.
53 The large tetragonal compression of the LS geometry results both from the short axial metal–ligand bonds imposed by the rigid structure of the tpy ligand and also,[6] from the superimposed elongation of the equatorial metal–ligand bonds due the strong Jahn–Teller instability which is operative in the ligand-field ^2E_g LS state.
54 I. B. Bersuker, *The Jahn–Teller Effect*, Cambridge University Press, Cambridge, 2006.
55 A. Vargas, PhD thesis, University of Geneva, 2009.
56 The experimental EPR data actually indicate that, in addition to the tetragonal ligand field, there is a weak rhombic distortion probably due to crystal packing.[6]
57 The fact that the spin crossover in $[Co(tpy)_2](ClO_4)_2{\cdot}1.3H_2O$ is not complete at room temperature[15] translates especially into an underestimation of the HS Co–N bond lengths. At a given temperature T, the observed Co–N bond lengths are indeed given by: $r_{HS} \times \gamma_{HS} + r_{LS} \times (1 - \gamma_{HS})$; where γ_{HS} is the HS fraction at T, and r_{HS} and r_{LS} the real values of the HS ($\gamma_{HS} = 1$) and LS ($\gamma_{HS} = 0$) bond lengths, respectively.
58 These configurations schematically read: $(3d_{xy})^2(3d_{xz})^1(3d_{yz})^2(3d_{x^2-y^2})^1(3d_{z^2})^1$ and $(3d_{xy})^2(3d_{xz})^2(3d_{yz})^1(3d_{x^2-y^2})^1(3d_{z^2})^1$, for the $^4B_1$ and $^4B_2$ states, respectively. Note that for the $^4A_2C_{2v}$ state, the configuration reads: $(3d_{xy})^1(3d_{xz})^2(3d_{yz})^2(3d_{x^2-y^2})^1(3d_{z^2})^1$.
59 Because of the dynamic nature of the PJT instability of the low-spin state, a correction should be added to its calculated zero-point energy.[54] However, this correction is expected to be a quite minor correction to the ground vibronic energy level of the low-spin state as given by $E^0(^2A_1)$ and is thus neglected.
60 A. Bolvin, *J. Phys. Chem. A*, 1998, **102**, 7525–7534.
61 H. Paulsen, L. Duelund, H. Winkler, H. Toftlund and A. X. Trautwein, *Inorg. Chem.*, 2001, **40**, 2201–2203.
62 A. Ghosh and P. R. Taylor, *Curr. Opin. Chem. Biol.*, 2003, **7**, 113–124.
63 J. N. Harvey, R. Poli and K. M. Smith, *Coord. Chem. Rev.*, 2003, **238–239**, 347–361.
64 A. Fouqueau, S. Mer, M. E. Casida, L. M. Lawson Daku, A. Hauser and T. Mineva, *J. Chem. Phys.*, 2004, **120**, 9473–9486.
65 R. J. Deeth and N. Fey, *J. Comput. Chem.*, 2004, **25**, 1840–1848.
66 H. Paulsen and A. X. Trautwein, in *Spin Crossover in Transition Metal Compounds II*, ed. P. Gütlich and H. A. Goodwin, Springer-Verlag, Heidelberg, 2004, vol. 235, pp. 197–219.
67 N. Kaltsoyannis, J. McGrady and J. Harvey, in *Principles and Applications of Density Functional Theory in Inorganic Chemistry I*, Springer-Verlag, Heidelberg, 2004, vol. 112, pp. 81–102.
68 M. Swart, A. R. Groenhof, A. W. Ehlers and K. Lammertsma, *J. Phys. Chem. A*, 2004, **108**, 5479–5483.
69 G. Ganzenmüller, N. Berkaïne, A. Fouqueau, M. E. Casida and M. Reiher, *J. Chem. Phys.*, 2005, **122**, 234321.
70 D. M. A. Smith, M. Dupuis and T. P. Straatsma, *Mol. Phys.*, 2005, **103**, 273–278.
71 L. M. Lawson Daku, A. Vargas, A. Hauser, A. Fouqueau and M. E. Casida, *ChemPhysChem*, 2005, **6**, 1393–1410.
72 A. Fouqueau, M. E. Casida, L. M. Lawson Daku, A. Hauser and F. Neese, *J. Chem. Phys.*, 2005, **122**, 044110.
73 A. Ghosh, *J. Biol. Inorg. Chem.*, 2006, **11**, 712–724.
74 A. Hauser, C. Enachescu, M. Lawson Daku, A. Vargas and N. Amstutz, *Coord. Chem. Rev.*, 2006, **250**, 1642–1652.
75 D. A. Scherlis, M. Cococcioni, P. Sit and N. Marzari, *J. Phys. Chem. B*, 2007, **111**, 7384–7391.
76 T. Guillon, L. Salmon, G. Molnár, S. Zein, S. Borshch and A. Bousseksou, *J. Phys. Chem. A*, 2007, **111**, 8223–8228.
77 S. Zein, S. A. Borshch, P. Fleurat-Lessard, M. E. Casida and H. Chermette, *J. Chem. Phys.*, 2007, **126**, 014105.
78 E. Tangen, J. Conradie and A. Ghosh, *J. Chem. Theory Comput.*, 2007, **3**, 448–457.
79 J. Conradie and A. Ghosh, *J. Chem. Theory Comput.*, 2007, **3**, 689–702.
80 I. H. Wasbotten and A. Ghosh, *Inorg. Chem.*, 2007, **46**, 7890–7898.
81 J. Conradie, T. Wondimagegn and A. Ghosh, *J. Phys. Chem. B*, 2008, **112**, 1053–1056.
82 K. Pierloot and S. Vancoillie, *J. Chem. Phys.*, 2008, **128**, 034104.
83 K. H. Marti, I. M. Ondík, G. Moritz and M. Reiher, *J. Chem. Phys.*, 2008, **128**, 014104.
84 K. P. Jensen, *Inorg. Chem.*, 2008, **47**, 10357–10365.
85 M. Swart, *J. Chem. Theory Comput.*, 2008, **4**, 2057–2066.
86 F. P. Rotzinger, *J. Chem. Theory Comput.*, 2009, **5**, 1061–1067.
87 K. P. Jensen and J. Cirera, *J. Phys. Chem. A*, 2009, **113**, 10033–10039.
88 A. Vargas, A. Hauser and L. M. Lawson Daku, *J. Chem. Theory Comput.*, 2009, **5**, 97–115.
89 J. Oláh and J. N. Harvey, *J. Phys. Chem. A*, 2009, **113**, 7338–7345.
90 L. M. Lawson Daku and A. Hauser, *J. Phys. Chem. Lett.*, 2010, **1**, 1830–1835.
91 S. Ye and F. Neese, *Inorg. Chem.*, 2010, **49**, 772–774.
92 H. Zhao, K. Pierloot, E. H. G. Langner, J. C. Swarts, J. Conradie and A. Ghosh, *Inorg. Chem.*, 2012, **51**, 4002–4006.
93 L. M. Lawson Daku and M. E. Casida, 2012, arXiv:1201.2398 [cond-mat.other].
94 K. P. Kepp, *Coord. Chem. Rev.*, 2013, **257**, 196–209.
95 L. Goerigk and S. Grimme, *Phys. Chem. Chem. Phys.*, 2011, **13**, 6670–6688.